Available online at www.sciencedirect.com

SCIENCE DIRECT®

Earth and Planetary Science Letters 235 (2005) 151–166

EPSL

www.elsevier.com/locate/epsl

The Late Devonian Frasnian–Famennian (F/F) biotic crisis: Insights from $\delta^{13}C_{carb}$, $\delta^{13}C_{org}$ and $^{87}Sr/^{86}Sr$ isotopic systematics

Daizhao Chen[a,*], Hairuo Qing[b], Renwei Li[a]

[a]*Institute of Geology and Geophysics, Chinese Academy of Sciences, P.O. Box 9825, Beijing 100029, China*
[b]*Department of Geology, University of Regina, Regina SK, Canada S4S 0A2*

Received 26 November 2004; received in revised form 3 March 2005; accepted 9 March 2005
Available online 23 May 2005
Editor: V. Courtillot

Abstract

A severe biotic crisis occurred during the Late Devonian Frasnian–Famennian (F/F) transition (±367 Myr). Here we present $\delta^{13}C_{carb}$, $\delta^{13}C_{org}$ and $^{87}Sr/^{86}Sr$ isotopic systematics, from identical samples of two sections across F/F boundary in South China, which directly demonstrate large and frequent climatic fluctuations (~200 kyr) from warming to cooling during the F/F transition. These climate fluctuations are interpreted to have been induced initially by increased volcanic outgassing, and subsequent enhanced chemical weathering linked to the rapid expansion of vascular plants on land, which would have increased riverine delivery to oceans and primary bioproductivity, and subsequent burial of organic matter, thereby resulting in climate cooling. Such large and frequent climatic fluctuations, together with volcanic-induced increases in nutrient (e.g., biolimiting Fe), toxin (sulfide) and anoxic water supply, and subsequent enhanced riverine fluxes and microbial bloom, were likely responsible for the stepwise faunal demise of F/F biotic crisis.

Keywords: $^{13}C/^{12}C$; $^{87}Sr/^{86}Sr$; Late Devonian; hydrothermal activity; climate change; vascular plant expansion; microbial bloom; mass extinction; South China

1. Introduction

The severe F/F biotic crisis, one of the greatest five in the Phanerozoic times, was characterized by stepwise massive demises by ~80% of marine fauna, particularly shallow-water tropical species

* Corresponding author. Tel.: +86 10 62008092; fax: +86 10 62010846.
E-mail address: dzh-chen@mail.iggcas.ac.cn (D. Chen).

0012-821X/$ - see front matter © 2005 Elsevier B.V. All rights reserved.
doi:10.1016/j.epsl.2005.03.018

[1]. Numerous hypotheses, including bolide impacts [2], marine anoxia [3] or land plant-induced marine anoxia [4,5], eutrophication [6], and climate warming [7] or cooling [8], have been proposed as the cause of this event. The ultimate cause of this extinction event, however, is still highly controversial.

A prominent feature of this event is the greatly increased $^{13}C/^{12}C$ ratios of marine carbonates ($\delta^{13}C_{carb}$) [3,9–11] and organic matter ($\delta^{13}C_{org}$) [6,9,10,12], indicating an increased burial rate of ^{13}C-depleted organic carbon (C_{org}) in response to the oceanic anoxia [3,10], and/or enhanced primary productivity [6]. Enhanced burial of organic matter would have, in turn, led to a significant drop in atmospheric CO_2 concentrations (or P_{CO_2}) [13], which may explain the apparent, transient climatic cooling, associated with the Late Kellwasser Event in the earliest Famennian [8]. Accordingly, the peak of $\delta^{13}C_{org}$ excursion should be larger in magnitude and later in time compared to $\delta^{13}C_{carb}$ values, as a result of a drop in the isotope fractionation effect (ε_p)—isotopic difference between aqueous dissolved CO_2 ($[CO_{2aq}]$) and biomass of marine phytoplankton [14,15]. However, such a pattern of $\delta^{13}C_{carb}$ and $\delta^{13}C_{org}$ pairs has not been established yet in the marine carbonates of Late Devonian in the global data set [3,6,9–12]; this has greatly limited our understanding of the oceanic and climatic changes over the F/F transition.

The Sr isotopic composition of seawater at any time represents the balance between continental weathering (radiogenic ^{87}Sr-enriched) and hydrothermal fluxes (^{87}Sr-depleted) to the oceans due to a short mixing time (~1500 years) and a long residence time (2~3 Myr.) of dissolved Sr in the oceans [16]. Increased continental weathering would increase the flux of both dissolved Sr with high $^{87}Sr/^{86}Sr$ ratios and nutrients to the oceans [17,18], causing an increase in oceanic primary productivity. Alternatively, increased sea-floor spreading, submarine volcanism, and hydrothermal activity would increase the flux of Sr with low $^{87}Sr/^{86}Sr$ ratios [19], as well as the flux of iron and reducing sulfide, thereby decreasing the oxygen content in bottom water. Therefore, the temporal variations of $^{87}Sr/^{86}Sr$ ratios of marine carbonates can reflect the signature and magnitude of interactions between tectonics, weathering rate and climate. Nevertheless, $^{87}Sr/^{86}Sr$ data across the F/F interval are extremely rare except for the low-resolution $^{87}Sr/^{86}Sr$ data sets presented by Veizer et al. [20].

In order to better constrain the tectonic, oceanic and climatic changes, and their biogeochemical responses during the F/F event, $\delta^{13}C_{carb}$–$\delta^{13}C_{org}$–$^{87}Sr/^{86}Sr$ isotopic systematics from identical sample sets of two sections across the F/F boundary in South China were analysed in this research; these combined isotopic data will provide more realistic information, greatly improving and refining our understanding of the causes of the F/F biotic crisis.

2. Geological setting

The Late Devonian carbonates were widely deposited on platforms and interplatform basins in the South China transtensional rift basin (Fig. 1A) [21]. The studied sections are located at Fuhe and Baisha between Guilin and Yangshuo, Guangxi province, South China. Palaeogeographically, they were located within the offshore spindle-shaped Yangshuo Basin, which was surrounded by shallow-water carbonate platforms and isolated from significant continental siliciclastic influxes (Fig. 1B). Such a basin configuration was interpreted as having been formed through strike-slip faulting [21]. The carbonates at these two localities are mainly composed of pelagic nodular limestones intercalated with subordinate calcareous gravity-flow deposits (calciturbidites and pebbly conglomerates), which are well dated through conodont zonation and high-resolution cyclostratigraphic approaches on the basis of Milankovitch orbital-forcing cyclicity (see Figs. 2 and 3) [22].

3. Materials and methods

Combined $\delta^{13}C_{carb}$, $\delta^{13}C_{org}$ and $^{87}Sr/^{86}Sr$ values were measured from identical samples from two sections (Fuhe and Baisha) (Fig. 1B) across the F/F boundary in South China. The analysed samples are micritic carbonates collected from basinal successions generally with a low

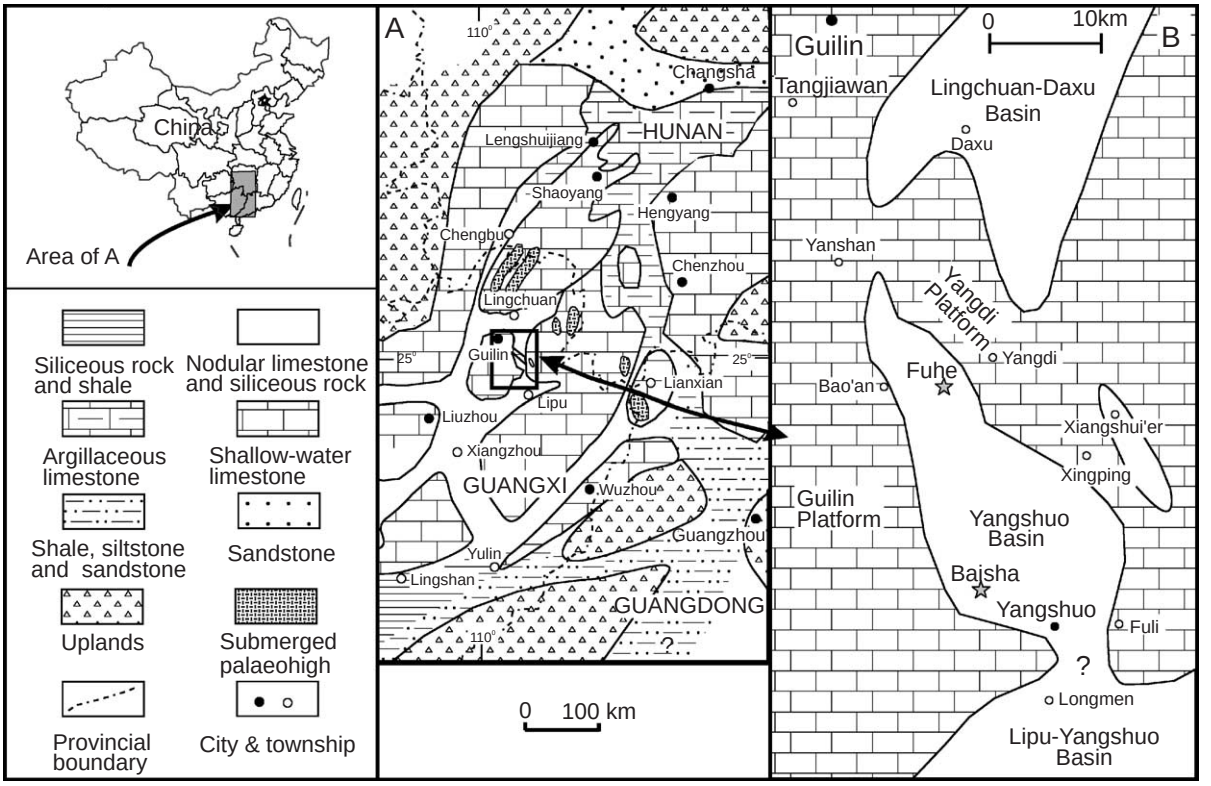

Fig. 1. Palaeogeographic setting of Guangxi and Hunan provinces in the Givetian–Frasnian (A) and detailed platform-basin configuration of Guilin region (B). Note the location and depositional context of studied sections (★) at Fuhe and Baisha.

content of organic matter (averaging ~0.05 wt.%, Fig. 2).

To minimise the degree to which the diagenesis may have obliterated the original isotopic signatures of the carbonates, detailed petrographic, cathodoluminescent microscopic and isotopic studies on the basinal carbonates were conducted; only non-luminescent, homogeneous micritic carbonates were selected for isotopic analyses. Powders (1–3 splits) were obtained from identical slabbed samples using a micro-drill (0.5–2.5 mm in diameter) after petrographic study. Sample splits (~5 mg) for carbon and oxygen analysis were reacted with 100% phosphoric acid at 50 °C for 24 h; isotopic ratios were measured on a Finnigan MAT-251 mass-spectrometer. Analytical precision is better than $\pm 0.05‰$ (1σ) both for $\delta^{13}C_{carb}$ and $\delta^{18}O$. Sample splits (300 mg to 1.5 g) for $\delta^{13}C_{org}$ analysis were first dissolved with 5 N HCl in a centrifuge beaker to remove carbonates through multiple acidification (at least two times) and subsequent drying in the heating oven, and repeatedly rinsed with deionized water to neutrality. The decalcified samples (30–110 mg)+1 g CuO wire were added to a quartz tube, then evacuated and sealed, and combusted at 500 °C for 1 h and at 850 °C for another 3 h. Isotopic ratios were analysed using cryogenically purified CO_2 on a Finnigan delta S mass spectrometer. Precision for $\delta^{13}C_{org}$ is better than $\pm 0.06‰$ (1σ). All stable isotope data were reported in standard δ-notation relative to Vienna Peedee Belmnite (VPDB) standard. Sample splits (1–5 mg) for strontium isotope analysis were digested in 2.5 N ultrapure HCl (1.5 ml) over night at room temperature. The strontium was extracted via 2.5

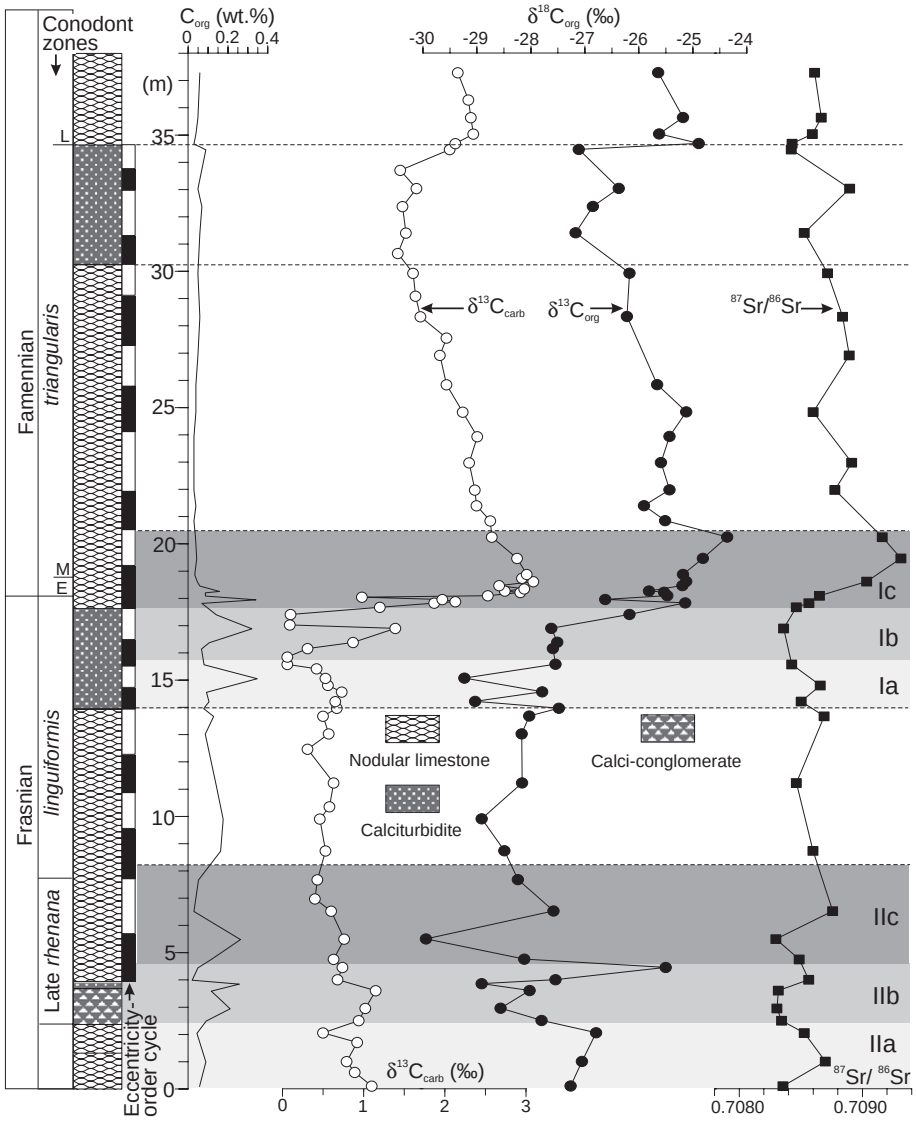

Fig. 2. Systematic variations of $\delta^{13}C_{carb}$, $\delta^{13}C_{org}$ and $^{87}Sr/^{86}Sr$ ratios from micritic carbonates across F/F transition at Fuhe. Vertical bars on the right side of lithological logs mark ranges of eccentricity-forcing depositional cycles (~100 kyr in duration), mainly based on the data of Chen and Tucker (2003) [22]. Shaded intervals (I and II) are mostly around the Upper and Lower Kellwasser Horizons, respectively, in which short-term fluctuations (spanning about two eccentricity cycles, ~200 kyr) in $\delta^{13}C_{carb}$, $\delta^{13}C_{org}$ and $^{87}Sr/^{86}Sr$ systematics are further identified (Ia–Ic and IIa–IIc).

ml ion exchange column (Biorad AGW50×8) in quartz glass and eluted with 2.5 N ultrapure HCl. Samples were analysed on a Finnigan MAT-262 multicollector thermal ionization mass-spectrometer (TIMS) with single Ta filament. NBS 987 standard was routinely measured for each batch of samples. The analytical mean error (2σ) is better than $\pm 15\times10^{-6}$ for $^{87}Sr/^{86}Sr$ ratios. All $^{87}Sr/^{86}Sr$ ratios were normalized relative to the nominal NBS 987 value (0.710240). Most of the

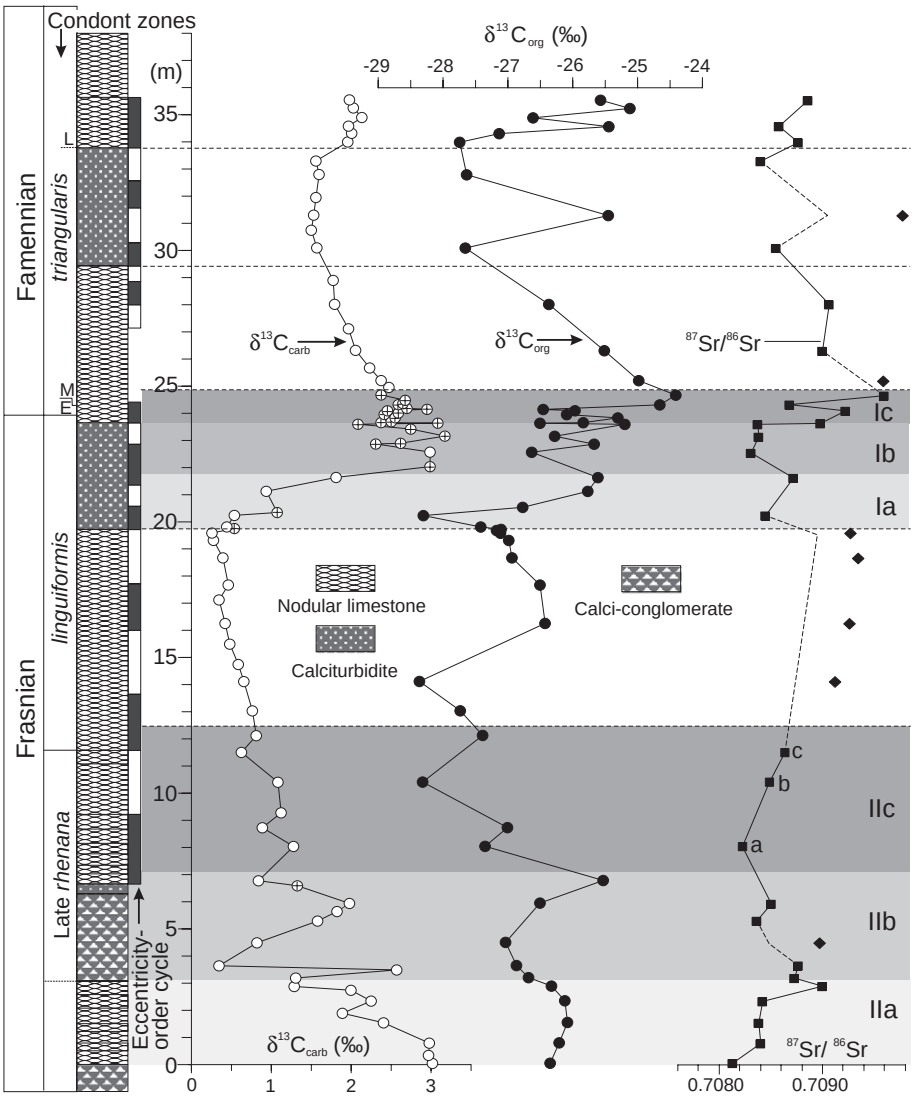

Fig. 3. Systematic variations of $\delta^{13}C_{carb}$, $\delta^{13}C_{org}$ and $^{87}Sr/^{86}Sr$ ratios of carbonate rocks across the F/F boundary at Baisha, South China. Samples with diamond symbols show covariance between $\delta^{18}O$ and $^{87}Sr/^{86}Sr$ values (see Fig. 5D), which may be influenced by diagenetic alteration. Crossed circles are $\delta^{13}C_{carb}$ data derived from Chen et al. (2002) [11]. Vertical bars on the right side of lithological logs mark ranges of eccentricity-forcing depositional cycles, mainly based on the data of Chen and Tucker (2003) [22]. Shaded horizons (I and II) are mostly around the Upper and Lower Kellwasser Horizons, respectively, in which short-term perturbations (~200 kyr) in $\delta^{13}C_{carb}$, $\delta^{13}C_{org}$ and $^{87}Sr/^{86}Sr$ values can also be identified (Ia–Ic and IIa–IIc). Note the highly condensed deposits in Ic, which may result in the loss of stratigraphic records.

samples were analysed at Ruhr University (Bochum) and some (for $\delta^{13}C_{carb}$ and $\delta^{18}O$, and $^{87}Sr/^{86}Sr$) were measured at the Institute of Geology and Geophysics, Chinese Academy of Science (Beijing) (Appendices A and B).

4. Results and evaluation

The systematic variations of $\delta^{13}C_{carb}$, $\delta^{13}C_{org}$ and $^{87}Sr/^{86}Sr$ values across the F/F boundary at Fuhe and Baisha are shown in Figs. 2 and 3, respectively. An

overall parallel positive excursion (interval I) of $\delta^{13}C_{carb}$ and $\delta^{13}C_{org}$ pairs, and $^{87}Sr/^{86}Sr$ ratios just across the F/F boundary, particularly at Fuhe, starts from the calciturbidite horizons (upper *linguiformis* zone) and ends in the base of nodular limestone successions (in the base of middle *triangularis* zone), spanning six eccentricity-driven depositional cycles (thereby spanning ~600 kyr) [22] (Figs. 2 and 3). This excursion is independent from the abundance of organic matter (see Fig. 2). Moreover, the magnitude and timing of the maximum $\delta^{13}C_{org}$ excursions is larger (~4.0–4.5‰) and later (~100 kyr) than those of $\delta^{13}C_{carb}$ excursions (~2.5‰), respectively (Figs. 2 and 3). Within this overall positive excursion, three shorter-term perturbations of isotopic variations, each spanning about two eccentricity cycles (~200 kyr), can be further identified (Ia–Ic, Figs. 2 and 3), in which the latest one (Ic) is temporally equivalent to the Upper Kellwasser Horizon [3]. The earlier two perturbations (Ia and Ib), which are confined within the calciturbidite horizon with a negative $^{87}Sr/^{86}Sr$ excursion, are characterized by slightly earlier shifts of $\delta^{13}C_{org}$ values, both negatively and positively, than $\delta^{13}C_{carb}$ values (Figs. 2 and 3). The latest perturbation (Ic), which is localized within the base of subsequent overlying nodular limestones (two eccentricity cycles) and the positive $^{87}Sr/^{86}Sr$ excursion, is characterized by concomitant positive excursions both in $\delta^{13}C_{carb}$ and $\delta^{13}C_{org}$ values, but with a larger and later maximum excursion of $\delta^{13}C_{org}$ values (Figs. 2 and 3).

Prior to the major excursion (I) described above, three short-term subordinate perturbations of $\delta^{13}C_{carb}$, $\delta^{13}C_{org}$ and $^{87}Sr/^{86}Sr$ values (herein named IIa to IIc), although not apparent as in interval I, can also be identified around upper *rhenana* conodont zone, which is approximately corresponding to the Lower Kellwasser Horizon [3], in which perturbation IIa is only partially included in this study (Figs. 2 and 3). These short-term perturbations generally start with negative shifts of $\delta^{13}C_{org}$ and $^{87}Sr/^{86}Sr$ ratios without obvious responses in $\delta^{13}C_{carb}$ values, which are followed by positive shifts in $\delta^{13}C_{org}$ and $^{87}Sr/^{86}Sr$ ratios either with no apparent responses of $\delta^{13}C_{carb}$ (IIc) or an early termination of increasing $\delta^{13}C_{carb}$ values (IIa and IIb).

Although the low organic content in the pelagic carbonates can reduce the possible diagenetic effects of C_{org} on $\delta^{13}C_{carb}$ signatures through organic decomposition and bacterial sulfate reduction during burial [9,13,23], it may enhance the diagenetic influences upon the $\delta^{13}C_{org}$ values [24–26]. However, at Fuhe, the well concomitant variations between $\delta^{13}C_{carb}$ and $\delta^{13}C_{org}$ values (Figs. 2 and 4A) are commonly considered as primary carbon isotopic signatures, as reported in many stratigraphic intervals [13,25–27], because diagenetic effects on the isotopic composition of carbonate and organic carbon are generally different [25]. In this case, the primary carbon isotopic signatures were basically well-preserved. The slight covariance between $\delta^{13}C_{carb}$ and $\delta^{18}O$ in the carbonates at Fuhe (Fig. 4B), on the other hand, possibly represents a primary signature, rather than a diagenetic imprint as commonly observed in carbonates [28–30]. No apparent covariance between $\delta^{18}O$ and $^{87}Sr/^{86}Sr$ values that both are sensitive to diagenetic alterations [28–30], suggest that their primary Sr isotopic signatures were well-preserved as well. The positive correlations between $^{87}Sr/^{86}Sr$, $\delta^{13}C_{carb}$ and $\delta^{13}C_{org}$ values from these carbonates (Fig. 4D, E) further point to a well-preserved, primary Sr isotopic signature, otherwise a negative correlation is commonly expected during diagenesis [28–30].

At Baisha, the covariance between $\delta^{13}C_{carb}$ and $\delta^{13}C_{org}$ values, although not good as at Fuhe, is generally clear (Figs. 3 and 5A), suggesting the preservation of primary carbon isotopic signatures [13,25–27]. No apparent covariance between $\delta^{13}C_{carb}$ and $\delta^{18}O$ values (Fig. 5B) suggests the primary signals of $\delta^{13}C_{carb}$ were minimally altered, likely in a closed system during burial [28–30]. Most samples show poor covariance between $\delta^{18}O$ and $^{87}Sr/^{86}Sr$ values (Fig. 5C), indicating a minimal alteration of primary Sr isotopic signatures in these samples. Nevertheless, the negative correlation between $^{87}Sr/^{86}Sr$ ratios and $\delta^{18}O$ values in some samples (Figs. 3 and 5D) suggest a likely diagenetic modification of $^{87}Sr/^{86}Sr$ ratios in these samples [28–30]. The slightly weaker correlations between $^{87}Sr/^{86}Sr$, $\delta^{13}C_{carb}$ and $\delta^{13}C_{org}$ values (Fig. 5E, F) compared with those at Fuhe (Fig. 4D, E) were also likely a response to diagenetic influences.

In general, isotopic signatures are better preserved at Fuhe than at Baisha. Both $\delta^{13}C_{carb}$ and $\delta^{13}C_{org}$ values are basically well preserved. Our $^{87}Sr/^{86}Sr$ data, particularly those at Fuhe, mimic the

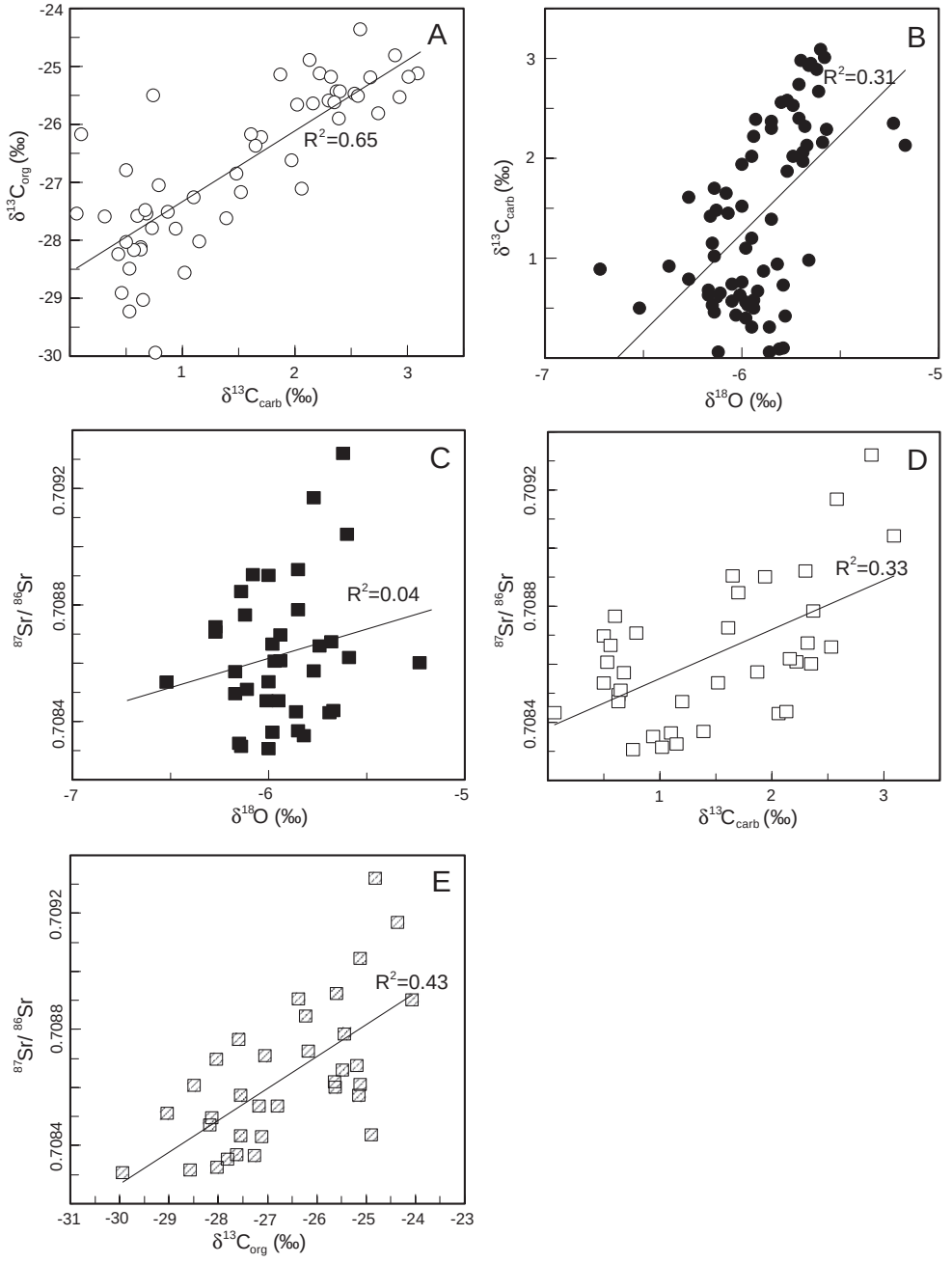

Fig. 4. Cross-plots between different isotopic values at Fuhe. (A) $\delta^{13}C_{org}$ vs. $\delta^{13}C_{carb}$; (B) $\delta^{13}C_{carb}$ vs. $\delta^{18}O$; (C) $^{87}Sr/^{86}Sr$ vs. $\delta^{18}O$; (D) $^{87}Sr/^{86}Sr$ vs. $\delta^{13}C_{carb}$; (E) $^{87}Sr/^{86}Sr$ vs. $\delta^{13}C_{org}$. All these criteria suggest well-preserved $\delta^{13}C_{carb}$, $\delta^{13}C_{org}$ and $^{87}Sr/^{86}Sr$ values (see the text for detailed documentation).

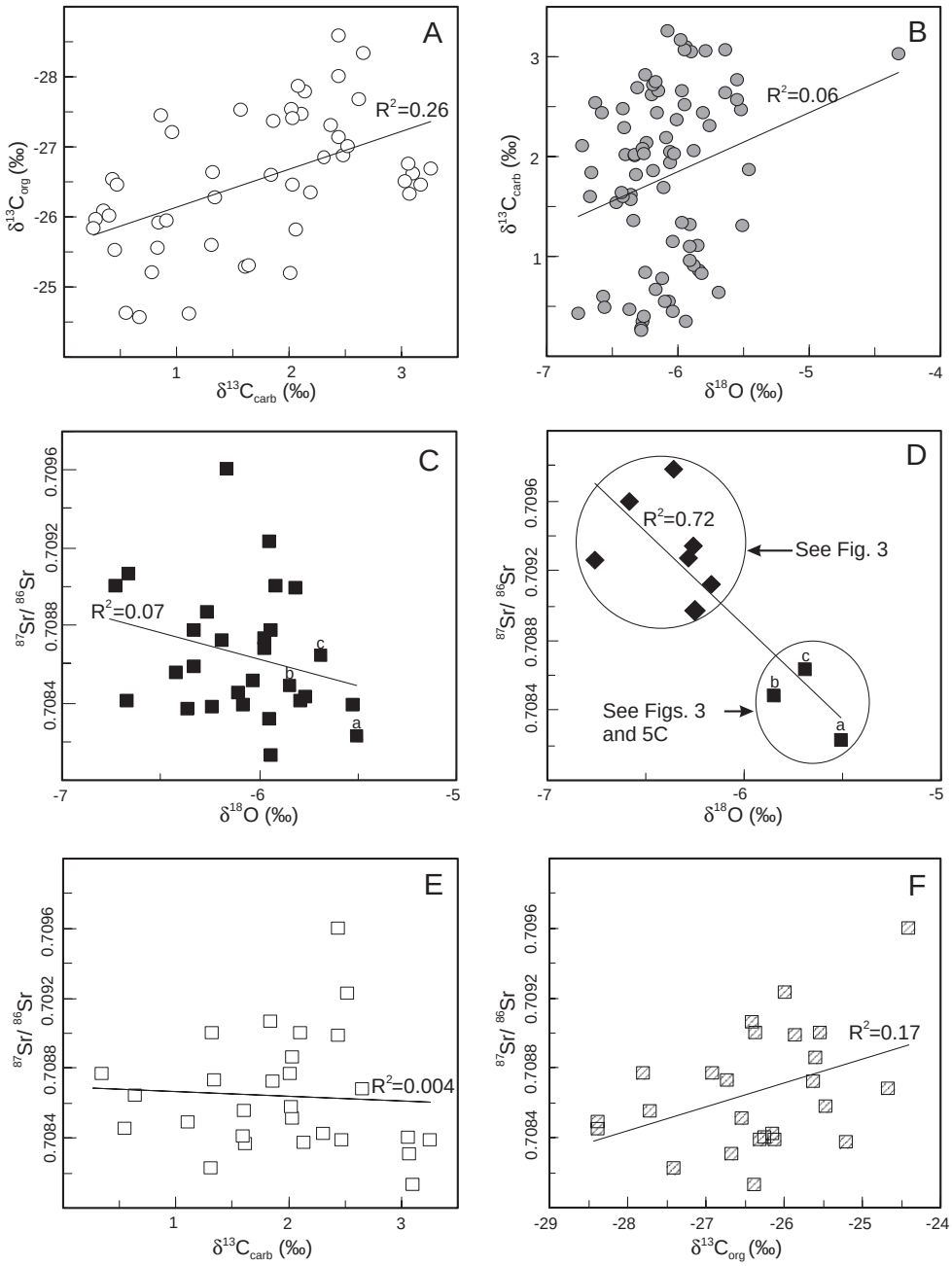

Fig. 5. Cross-plots between different isotopic values at Baisha. (A) $\delta^{13}C_{org}$ vs. $\delta^{13}C_{carb}$; (B) $\delta^{13}C_{carb}$ vs. $\delta^{18}O$; (C) $^{87}Sr/^{86}Sr$ vs. $\delta^{18}O$ for most samples; (D) $^{87}Sr/^{86}Sr$ vs. $\delta^{18}O$ for a part of samples, in which the samples with diamond symbols may have influenced by diagenesis; (E) $^{87}Sr/^{86}Sr$ vs. $\delta^{13}C_{carb}$ for most samples as illustrated in (C); (F) $^{87}Sr/^{86}Sr$ vs. $\delta^{13}C_{org}$ for most samples as illustrated in (C).

trend of $^{87}Sr/^{86}Sr$ ratios from well-preserved brachiopods from Germany for the same time interval [20], also suggesting the preservation of general trend of $^{87}Sr/^{86}Sr$ variations in our micrite samples, although a systematic difference may exist between analysed micrites and brachiopods [31].

5. Discussions

Isotope values of well-preserved micrites generally reveal a prominent overall positive excursion (interval I) in $\delta^{13}C_{carb}$, $\delta^{13}C_{org}$ and $^{87}Sr/^{86}Sr$ values (Figs. 2,3). Such a variation pattern of $\delta^{13}C_{carb}$–$\delta^{13}C_{org}$ pairs with concomitant increase of $^{87}Sr/^{86}Sr$ ratios from identical sections, to our knowledge, has not been reported from the F/F transition in earlier studies [3,6,9–11]. Although a similar pattern of $\delta^{13}C_{carb}$ and $\delta^{13}C_{org}$ pairs from identical sections across the F/F boundary has been reported by Joachimski et al. [12], nevertheless the $\delta^{13}C_{carb}$ values have been lately proven to have been apparently influenced by diagenetic alteration due to a high organic content [9]. It seems, in such short intervals of measured sections in the present study, nearly the same diagenetic and geothermal conditions during burial were unlikely to account for such a large excursion of $\delta^{13}C_{org}$. The organic matter is exclusively of marine biomass, particularly at Fuhe, which is overwhelmingly composed of short-chain *n*-alkanes (with no apparent odd-over-even carbon number predominance) contributed by phytoplankton, and rare isoprenoids of bacterial/algal origin [32]. This further precludes other possible biomass sources (i.e., terrestrial plants richer in ^{13}C) being responsible for the positive $\delta^{13}C_{org}$ excursion. All these suggest that this excursion was a primary signal of oceanic and biogeochemical perturbations.

Examining the early stage of the overall positive excursion (I), two short-term (~200 kyr) negative-to-positive perturbations (Ia and Ib), with an early onset of $\delta^{13}C_{org}$ shift relative to $\delta^{13}C_{carb}$ values, are further identified (Figs. 2 and 3). The short-term negative shifts (particularly the earliest one) of $\delta^{13}C_{org}$ values with delayed responses of $\delta^{13}C_{carb}$ data may have been resulted from climatic warming [15], which would influence the atmospheric Pco_2 level, thereby the $[CO_{2aq}]$ in the surface seawater. Since $[CO_{2aq}]$ comprises only a small fraction of total dissolved inorganic carbon (DIC) in the ocean, a short-term climatic warming can influence the $\delta^{13}CO_{2aq}$ (thereby $\delta^{13}C_{org}$), but has no immediate effect on $\delta^{13}C_{DIC}$ or $\delta^{13}C_{carb}$ values [14,15]. The subsequent earlier onset of positive shifts in $\delta^{13}C_{org}$ values with respect to $\delta^{13}C_{carb}$ values, however, may reflect a decrease in isotopic fractionation between $[CO_{2aq}]$ and biomass of marine phytoplankton due to a drop in temperature of the surface water [14,15], likely a result of short-term climatic cooling. Such short-term climatic fluctuations may have been related to the intensity of volcanic (or hydrothermal) outgassing. The decreased$^{87}Sr/^{86}Sr$ ratios within Ia and Ib intervals (Figs. 2 and 3) and their equivalent in Germany [20] support the assumption of enhanced volcanic-hydrothermal activities [19]. Coeval intense volcanic activities were widely reported in eastern Laurussia, Kazakhstan-Tianshan and Eurasia, particularly in the East Europe where strongly rifting volcanism occurred [33,34] and in Siberia where the "Viluy trap" was recently dated to the F/F transitional period [35]. In South China, extensive bedded cherts and tuffaceous fallouts (locally with eruptive pillow lavas) induced by hydrothermal activity, although culminating in the early Frasnian [21], persisted into the middle Famennian [36]. The bloom of silica-secreting fauna across the F/F boundary also supports enhanced volcanic-hydrothermal activity [37]. All these reduce the possibility of species-specific isotopic effects on the discrimination between $\delta^{13}C_{carb}$ and $\delta^{13}C_{org}$ pairs [38]. The volcanically-generated CO_2 is generally considered to be resident in the air for ~10^5 years (~200 kyr) [15,39], thus multiple short-term volcanic outgassing (during Ia and Ib) could have cumulatively led to a significant rise in atmospheric Pco_2 levels, thereby driving towards a significant climatic warming [39] and a significant rise in sea-level [11,22] in the latest Frasnian time (the earliest Ic, Figs. 2 and 3).

In the late stage of the major excursion (Ic), equivalent to the Late Kellwasser Event [3], the concomitant increase of $\delta^{13}C_{carb}$, $\delta^{13}C_{org}$ and $^{87}Sr/^{86}Sr$ values with a larger and slightly delayed $\delta^{13}C_{org}$ peak (~100 kyr) (Figs. 2 and 3), for the first

time, provides the direct evidence that the enhanced burial of organic matter could have been linked to increased chemical weathering and subsequent riverine delivery to oceans; both led to enhanced sequestration of atmospheric CO_2, thereby resulting in apparent climatic cooling. The apparent climatic warming in the early stage of Ic, as discussed above, could have reinforced the hydrological cycle [17], accelerated the expansion of vascular plants into uplands and subsequently enhanced chemical weathering [4,5,40], thereby leading to increased continental runoff and riverine nutrient flux to oceans [15,17,18]. These, in turn, could have enhanced the primary productivity and subsequent organic burial rate in marine basins, leading to simultaneous increases both in $\delta^{13}C_{carb}$ and $\delta^{13}C_{org}$ values [15,41], as observed in this study (Figs. 2 and 3). However, accelerated weathering and burial consumption of atmospheric CO_2 without continuous compensation of volcanic-released CO_2 would have finally led to the lowering of Pco_2 levels and apparent climatic cooling, as reflected by the later appearance and larger magnitude of $\delta^{13}C_{org}$ maximum (Figs. 2 and 3) due to a decrease in photosynthetic carbon fixation of marine phytoplankton [15]. This climatic cooling is also supported by the oxygen isotopic data from the Europe [8]. Mass-balance modelling suggests that such a variation of $\delta^{13}C_{carb}$ and $\delta^{13}C_{org}$ pairs, with a later appearance and a larger magnitude of $\delta^{13}C_{org}$ maximum, could only occur when Pco_2 levels were lower than 10 times of pre-industrial Pco_2 values (e.g.,<~3000 ppmv) [15]. This implies that the Pco_2 level during the early Late Devonian time may have not been so high, as suggested by other authors (generally $\geq$3000 ppmv) [12,42]. This climatic scenario is further supported by independent evidence from pedogenic carbonates from which the atmospheric Pco_2 level of the Late Devonian was estimated about 4–6 times of pre-industrial level (1200–1800 ppmv) [43–45]. After the major excursion in the early Famennian, $\delta^{13}C_{carb}$, $\delta^{13}C_{org}$ and $^{87}Sr/^{86}Sr$ ratios decreased concurrently, but stabilized at slightly higher values compared to the pre-event values (Figs. 2 and 3); this may reflect a reduced silicate weathering at high-latitudes, buffered by enhanced carbonate weathering at low-latitudes [15] during sea-level fall [11,22].

Three short-term subordinate perturbations (each ~200 kyr in period) of $\delta^{13}C_{carb}$, $\delta^{13}C_{org}$, and $^{87}Sr/^{86}Sr$ systematics (IIa to IIc) are present prior to the major excursion (I); they generally start with apparent negative shifts of $\delta^{13}C_{org}$ and $^{87}Sr/^{86}Sr$ ratios without obvious responses in $\delta^{13}C_{carb}$ values, which are then followed by positive shifts in $\delta^{13}C_{org}$ and $^{87}Sr/^{86}Sr$ ratios either with no apparent responses of $\delta^{13}C_{carb}$ (IIc) or an early termination of increasing $\delta^{13}C_{carb}$ values (IIa and IIb) (Figs. 2 and 3), similar to the variation patterns of Ia and Ib perturbations described above. Accordingly, all these shifts suggest the volcanic-hydrothermal activity as a causal mechanism responsible for the variations of $\delta^{13}C_{carb}$, $\delta^{13}C_{org}$, and $^{87}Sr/^{86}Sr$ systematics, as discussed above. However, only high enough emanation of volcanic CO_2 into the atmosphere, allowing to reside for a reasonable time interval, could the chemical weathering and riverine nutrient flux have been enhanced significantly, leading to an apparent increase in primary productivity and organic burial rate, and a subsequent decrease in Pco_2 level (or climatic cooling), thereby positive shifts both in $\delta^{13}C_{carb}$ and $\delta^{13}C_{org}$ values (i.e., perturbations IIa and IIb), with a delayed but larger maximum for the latter (Figs. 2 and 3).

The isotopic difference between carbonate and organic carbon ($\Delta^{13}C = \delta^{13}C_{carb} - \delta^{13}C_{org}$) is not only an indicator of primary isotope composition of carbon, but also a reflection of carbon isotopic fractionation (ε_p) of marine phytoplankton [25,26], which is considered mainly a function of $[CO_{2aq}]$ or atmospheric Pco_2 level [14,15,46], particularly when the $[CO_{2aq}]$ is above a critical concentration (i.e., >10 μmol/kg) [47], although it may also relate to other factors, i.e., species, cell geometry and growth rate of marine biomasses [38,48]. The high atmospheric Pco_2 level during the early Late Devonian time, as documented above, could have readily resulted in a $[CO_{2aq}]$ higher than the threshold concentration in the surface seawater according to Henry's Law; thus the systematic variations of $\Delta^{13}C$ could be also used as a proxy of changes in atmospheric Pco_2 level, thereby revealing the climatic changes [14,15]. In this study, $\Delta^{13}C$ values are very constant ($28.2 \pm 2.5‰$) both

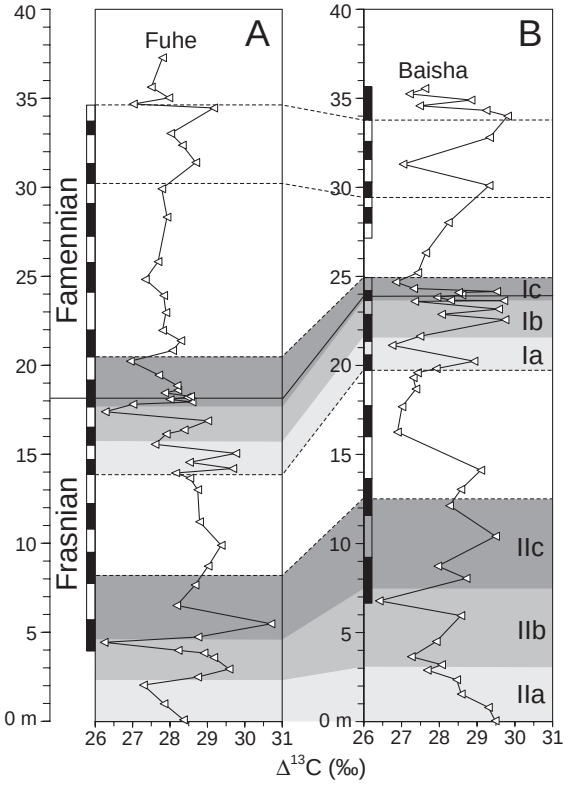

Fig. 6. Systematic variations in $\Delta^{13}C$ values ($=\delta^{13}C_{carb}-\delta^{13}C_{org}$) across F/F boundary for studied sections at Fuhe (A) and Baisha (B). Apparent fluctuations of $\Delta^{13}C$ values, reflecting perturbations of isotopic differences between deposited carbonates and marine biomasses [24,25], occur in both intervals I and II, particularly in the upper one. Vertical bars represent the range of eccentricity-forcing depositional cycles (~100 kyr) as in Figs. 2 and 3. Note the highly condensed deposits in the base of Ic at Fuhe.

at Fuhe and Baisha (Appendices A and B), suggesting that the primary carbon isotopic signatures were well preserved [25,27]. Examining the systematic $\Delta^{13}C$ variations for the whole studied sections at Fuhe and Baisha, it is interesting to note that three fluctuations of $\Delta^{13}C$ values (each spanning ~200 kyr) cluster around interval I (just across the F/F boundary) and interval II (the horizon equivalent to the Lower Kellwasser Horizon), respectively (Fig. 6). These short-term perturbations of $\Delta^{13}C$ variations, generally with magnitudes of 1.5–4.5‰, thus suggest large and frequent fluctuations of Pco_2 level [14,15], accordingly large and frequent climatic fluctuations from warming to cooling in a time shorter than 100 kyr during the F/F transition (Fig. 6).

Our isotopic data of $\delta^{13}C_{carb}$, $\delta^{13}C_{org}$, and $^{87}Sr/^{86}Sr$ systematics suggest that the large and frequent climatic fluctuations, occurring mostly around the equivalent Lower and Upper Kellwasser horizons, respectively, were initially triggered by enhanced volcanic (or hydrothermal) activity during the F/F transition. These short-term climatic changes could have readily influenced the sea-surface temperatures (SST), but exerted no substantial influences on the temperature of deep-water columns. This scenario could have resulted in severe ecological stresses on those shallow-water benthic dwellers to adjust their physiology to such frequent climatic 'mega-burps', thereby inhibiting the origination of new species and their radiation [49]. In the meantime, such climatic fluctuations, together with a significant boost in volcanic-supplied nutrients (e.g., bio-limiting Fe, Zn), toxin (or sulfide), anoxic water supply, and subsequent riverine influxes to oceans, as discussed above, could have promoted microbial bloom in shallow seawater [50], as widely observed worldwide at the F/F boundary [1]. The microbial bloom could have not only poisoned the ecological condition for shallow-water fauna, but also rapidly invaded and occupied the ecological niches where the shallow-water benthic dwellers used to be colonized mainly due to competition [51]. All these factors finally led to their step-down massive demise during the F/F transition. The fact of rapid, episodic climate changes reconcile well the stepwise massive faunal demise during the F/F transition [1].

Acknowledgements

We thank B.A. Yin for field assistance, and Ulrike Schulte (Bochum) and F.S. Zhang (Beijing) for isotope analyses. This work was supported by the National Natural Science Foundation of China (Grant NO. 40372062) for D.C. and by the NSERC Discovery Grant 155012 for H.Q. Constructive comments from J. Veizer and T. Algeo, and editorial help from V. Courtillot are greatly appreciated.

Appendix A. Summary table of TOC, isotopic data and $\Delta^{13}C$ values at Fuhe

Samples	Height (m)	Lithology	TOC	$\delta^{13}C_{carb}$	$\delta^{13}O$	$\delta^{13}C_{org}$	$^{87}Sr/^{86}Sr$ (2σ)	$\Delta^{13}C$
FH′-1	0.1	NL	0.06	1.10	−5.98	−27.26	0.708356 ± 6	28.36
FH′-2	0.6	NL		0.89	−6.72			
FH′-3	1	NL	0.09	0.79	−6.27	−27.05	0.708700 ± 6	27.84
FH′-4	1.7	NL		0.92	−6.37			
FH′-5	2.05	NL	0.05	0.50	−6.52	−26.79	0.708528 ± 6	27.29
FH′-6	2.5	CC	0.09	0.94	−5.82	−27.8	0.708344 ± 6	28.74
FH′-7	2.95	CC	0.21	1.02	−6.14	−28.56	0.708307 ± 6	29.58
FH′-9	3.6	CC	0.12	1.15	−6.15	−28.02	0.708318 ± 6	29.17
F126	3.85	CT	0.26			−28.91		28.91
FH′10	4	NL	0.02	0.68	−6.17	−27.54	0.708564 ± 6	28.22
FH′11	4.45	NL	0.05	0.74	−6.05	−25.5		26.24
FH′12	4.75	NL	0.12	0.63	−6.17	−28.12	0.708488 ± 6	28.75
FH′14	5.49	NL	0.26	0.76	−6.00	−29.94	0.708298 ± 6	30.70
FH′16	6.52	NL	0.03	0.60	−6.12	−27.58	0.708758 ± 6	28.18
FH′17	6.97	NL		0.40	−5.98			
F131	7.67	NL	0.05	0.43	−6.03	−28.24		28.67
FH′20	8.73	NL	0.16	0.53	−5.97	−28.49	0.708600 ± 6	29.02
FH′22	9.9	NL	0.18	0.46	−6.14	−28.91		29.37
FH′24	11.22	NL	0.14	0.63	−6.01	−28.16	0.708464 ± 6	28.79
FH′26	12.46	NL		0.31	−5.95			
FH′27	13.02	NL	0.09	0.57	−6.05	−28.17		28.74
FH′28	13.67	NL	0.13	0.50	−5.94	−28.03	0.708690 ± 6	28.53
FH′28*		NL					*0.708551 ± 15*	
FH′29	13.96	NL	0.08	0.67	−5.92	−27.48		28.15
FH′30	14.21	NL	0.11	0.65	−6.11	−29.03	0.708503 ± 6	29.68
FH′31	14.56	CT	0.09	0.73	−5.79	−27.79		28.52
FH′32	14.8	CT		0.56	−5.98		0.708658 ± 13	
FH′33	15.06	CT	0.35	0.53	−6.15	−29.23		29.76
FH′34	15.41	CT		0.42	−5.78			
FH′35	15.57	CT	0.08	0.06	−5.86	−27.54	0.708426 ± 6	27.60
FH′36	15.84	CT		0.06	−6.12			
FH′37	16.15	CT	0.07	0.31	−5.86	−27.59		27.90
FH′38	16.38	CT	0.11	0.87	−5.89	−27.51		28.38
FH′39	16.89	CT	0.32	1.39	−5.85	−27.62	0.708361 ± 6	29.01
FH′40	17.02	CT		0.09	−5.81			
FH′41	17.4	CT	0.14	0.10	−5.79	−26.17		26.27
FH′42	17.67	CT		1.20	−5.95		0.708464 ± 6	
FH′43	17.82	NL	0.07	1.87	−5.77	−25.14	0.708566 ± 6	27.01
FH′44	17.87	NL		2.13	−5.17			
FH′45	17.95	NL	0.34	1.97	−5.69	−26.62		28.59
FH′46	18.04	NL		0.98	−5.66			
FH′47	18.09	NL	0.09	2.53	−5.74	−25.47	0.708652 ± 6	28.00
FH′48	18.21	NL	0.09	2.93	−5.66	−25.53		28.46
FH′49	18.26	NL	0.16	2.74	−5.71	−25.81		28.55
FH′50	18.34	NL		2.98	−5.70			
FH′51	18.46	NL	0.06	2.67	−5.61	−25.19		27.86
FH′52	18.61	NL	0.05	3.09	−5.60	−25.12	0.709035 ± 6	28.21
FH′53	18.73	NL		2.95	−5.65			
FH′54	18.87	NL	0.03	3.01	−5.58	−25.18		28.19
FH′55	19.46	NL	0.04	2.89	−5.62	−24.81	0.709313 ± 6	27.70
FH′56	20.24	NL	0.04	2.58	−5.77	−24.36	0.709161 ± 6	26.94
FH′55*		NL	*0.04*	*3.00*	*−5.83*		*0.708988 ± 12*	

Appendix A *(continued)*

Samples	Height (m)	Lithology	TOC	$\delta^{13}C_{carb}$	$\delta^{13}O$	$\delta^{13}C_{org}$	$^{87}Sr/^{86}Sr$ (2σ)	$\Delta^{13}C$
FH′56*		NL	*0.03*	*2.85*	*−5.80*		*0.708857 ± 10*	
FH′57	20.84	NL	*0.03*	*2.56*	*−5.80*	−25.51		28.07
FH′59	21.39	NL	*0.04*	*2.39*	*−5.93*	−25.90		28.29
FH′60	21.97	NL	*0.03*	*2.37*	*−5.85*	−25.43	*0.708776 ± 13*	27.80
FH′62	22.97	NL	*0.03*	*2.30*	*−5.85*	−25.59	*0.708914 ± 13*	27.89
FH′64	23.93	NL	*0.03*	*2.40*	*−5.71*	−25.43		27.83
FH′66	24.83	NL	*0.04*	*2.22*	*−5.94*	−25.12	*0.708601 ± 13*	27.34
FH′68	25.83	NL	*0.04*	*2.02*	*−5.74*	−25.66		27.68
FH′70	26.91	NL	*0.05*	*1.94*	*−6.00*		*0.708894 ± 14*	
FH′72	27.55	NL		*2.02*	*−5.95*			
FH′74	28.33	NL	*0.06*	*1.70*	*−6.14*	−26.22	*0.708839 ± 13*	27.92
FH′75	29.08	NL		*1.64*	*−6.08*			
FH′76	29.92	NL	*0.05*	*1.61*	*−6.27*	−26.17	*0.708718 ± 12*	27.78
FH′77	30.65	CT		*1.42*	*−6.16*			
FH′78	31.4	CT	*0.06*	*1.52*	*−6.00*	−27.17	*0.708529 ± 12*	28.69
FH′79	32.37	CT	*0.07*	*1.48*	*−6.13*	−26.85		28.33
FH′81	33.03	CT	*0.05*	*1.65*	*−6.08*	−26.37	*0.708897 ± 12*	28.02
FH′82	33.7	CT		*1.45*	*−6.07*			
FH′84	34.46	CT	*0.09*	*2.06*	*−5.69*	−27.11	*0.708423 ± 12*	29.17
FH′85	34.68	NL	*0.03*	*2.13*	*−5.67*	−24.89	*0.708430 ± 12*	27.02
FH′86	35.03	NL	*0.04*	*2.35*	*−5.23*	−25.62	*0.708594 ± 13*	27.97
FH′88	35.63	NL	*0.05*	*2.32*	*−5.68*	−25.18	*0.708666 ± 14*	27.50
FH′89	36.28	NL		*2.29*	*−5.57*			
FH′90	37.28	NL	*0.06*	*2.16*	*−5.59*	−25.64	*0.708612 ± 13*	27.80

TOC-total organic carbon (wt.%). Stable isotope data are reported in per mil relative to VPDB, $\Delta^{13}C = \delta^{13}C_{carb} - \delta^{13}C_{org}$. Sr isotopic ratios are normalized to NBS 987 standard of 0.710240. NL—nodular limestone, CT—calciturbidite, CC—calci-conglomerate. Data in normal font were analysed at Ruhr University (Bochum), those in italics were measured at Institute of Geology and Geophysics, CAS (Beijing); *—interlab checking.

Appendix B. Summary table of isotopic data and $\Delta^{13}C$ values at Baisha

Samples	Height (m)	Lithology	$\delta^{13}C_{carb}$	$\delta^{13}O$	$\delta^{13}C_{org}$	$^{87}Sr/^{86}Sr$ (2σ)	$\Delta^{13}C$
Bs′-1	0.05	NL	*3.10*	*−5.94*	−26.38	*0.708130 ± 13*	29.48
Bs′-2	0.35	NL	*3.05*	*−5.90*			
Bs′-3	0.8	NL	*3.06*	*−5.79*	−26.24	*0.708402 ± 13*	29.30
Bs′-6	1.55	NL	*2.47*	*−5.52*	−26.11	*0.708389 ± 13*	28.58
Bs′-7	1.9	NL	*1.94*	*−6.06*			
Bs′-9	2.35	CT	*2.31*	*−5.76*	−26.15	*0.708422 ± 13*	28.46
Bs′-10	2.75	NL	*2.05*	*−6.06*			
Bs′-11	2.89	NL	*1.32*	*−5.91*	−26.36	*0.709002 ± 13*	27.68
Bs′-12	3.2	CC	*1.34*	*−5.97*	−26.72	*0.708729 ± 14*	28.06
Bs′-13	3.5	CC	*2.64*	*−5.64*			
Bs′-14	3.65	CC	*0.35*	*−5.94*	−26.91	*0.708770 ± 13*	27.26
Bs′-16	4.5	CC	*0.84*	*−6.25*	−27.08	*0.708974 ± 13*	27.92
Bs′-18	5.3	CC	*1.62*	*−6.36*		*0.708365 ± 13*	
Bs′-19	5.65	CC	*1.87*	*−5.46*			
Bs′-20	5.95	CC	*2.03*	*−6.03*	−26.54	*0.708509 ± 13*	28.57

(continued on next page)

Appendix B (*continued*)

Samples	Height (m)	Lithology	$\delta^{13}C_{carb}$	$\delta^{13}O$	$\delta^{13}C_{org}$	$^{87}Sr/^{86}Sr$ (2σ)	$\Delta^{13}C$
Bs-1	6.6	CT	**1.36**	**−6.34**			
Bs′-21	6.785	NL	*0.86*	*−5.84*	−25.55		26.41
Bs′-24	8.045	CT	*1.31*	*−5.51*	−27.40	*0.708226 ± 14*	28.71
Bs′-25	8.735	NL	*0.91*	*−5.88*	−27.05		27.96
Bs′-26	9.285	NL	*1.15*	*−6.04*			
Bs′-28	10.41	NL	*1.11*	*−5.85*	−28.38	*0.708490 ± 13*	29.49
Bs′-28′	11.51	CT	*0.64*	*−5.69*		*0.708641 ± 15*	
Bs′-28+	12.13	NL	*0.83*	*−5.82*	−27.44		28.27
Bs′-29	13.04	NL	*0.78*	*−6.12*	−27.79		28.57
Bs′-31	14.12	NL	*0.67*	*−6.17*	−28.43	*0.709118 ± 13*	29.10
Bs′-32	14.75	NL	*0.60*	*−6.57*			
Bs′-33	15.5	NL	*0.49*	*−6.56*			
Bs′-34	16.26	NL	*0.43*	*−6.76*	−26.46	*0.709258 ± 12*	26.89
Bs′-35	17.13	NL	*0.35*	*−6.27*			
Bs′-37	17.68	NL	*0.47*	*−6.37*	−26.54		27.01
Bs′-39	18.68	NL	*0.40*	*−6.26*	−26.98	*0.709342 ± 14*	27.38
Bs′-40	19.32	NL	*0.28*	*−6.28*	−27.03		27.31
Bs′-41	19.59	NL	*0.26*	*−6.28*	−27.16	*0.709274 ± 13*	27.42
Bs′-41a	19.69	Sh			−27.22		
Bs-41b	19.73	Sh			−27.15		
Bs3	19.76	NL	**0.55**	**−6.07**			
Bs′-42	19.82	CT	*0.45*	*−6.04*	−27.47		27.92
Bs′-44	20.24	CT	*0.55*	*−6.10*	−28.37	*0.708413 ± 12*	28.92
Bs4	20.345	CT	**1.10**	**−5.91**			
Bs′-45	20.54	Sh M			−26.81		
Bs′-46	21.13	CT	*0.96*	*−5.91*	−25.79		26.75
Bs′-47	21.64	CT	*1.86*	*−6.19*	−25.63	*0.708719 ± 13*	27.49
Bs-6	22.04	CT	**3.07**	**−5.64**			
Bs′-49	22.57	CT	*3.07*	*−5.95*	−26.67	*0.708309 ± 12*	29.74
Bs-7	22.87	CT	**2.37**	**−6.01**	−25.69		28.06
Bs-8	22.9	CT	**2.69**	**−6.31**			
Bs-9	23.16	CT	**3.26**	**−6.08**	−26.31	*0.708388 ± 13*	29.57
Bs-10	23.42	CT	**2.82**	**−6.25**			
Bs-11	23.6	CT	**2.14**	**−6.24**	−25.21	*0.708375 ± 14*	27.35
Bs-12	23.64	Sh M	**3.17**	**−5.98**	−26.54		29.71
BS-13	23.66	NL	**2.44**	**−5.81**	−25.86	*0.708984 ± 13*	28.30
BS-13+	23.69	NL	**2.57**	**−5.55**			
BS-14	23.84	NL	**2.62**	**−6.20**	−25.32		27.94
BS-15	23.96	Sh M	**2.48**	**−6.42**	−26.12		28.60
BS-16b	24.01	NL	**2.66**	**−6.15**			
BS-16t	24.1	NL	**2.52**	**−5.95**	−25.99	*0.709228 ± 14*	28.51
BS-17	24.15	Sh M	**3.03**	**−4.32**	−26.49		29.52
BS-18	24.18	NL	**2.77**	**−5.55**			
BS-19	24.32	NL	**2.66**	**−5.97**	−24.66	*0.708680 ± 12*	27.32
BS-20	24.36	NL	**2.72**	**−6.19**			
BS-21	24.48	NL	**2.75**	**−6.17**			
BS-22	24.68	NL	**2.44**	**−6.16**	−24.41	*0.709602 ± 13*	26.85
BS′-50	24.96	NL	*2.54*	*−6.63*			
BS′-51	25.21	NL	*2.44*	*−6.58*	−24.99	*0.709592 ± 13*	27.43
BS′-52	25.67	NL	*2.29*	*−6.41*			
BS′-53	26.32	NL	*2.11*	*−6.73*	−25.53	*0.708998 ± 14*	27.64
BS′-54	27.12	NL	*2.02*	*−6.40*			
BS′-55	28.02	NL	*1.84*	*−6.66*	−26.40	*0.709063 ± 14*	28.24
BS′-56	28.9	NL	*1.82*	*−6.32*			

Appendix B *(continued)*

Samples	Height (m)	Lithology	$\delta^{13}C_{carb}$	$\delta^{13}O$	$\delta^{13}C_{org}$	$^{87}Sr/^{86}Sr$ (2σ)	$\Delta^{13}C$
BS′-57	30.1	NL	*1.61*	*−6.42*	−27.71	*0.708552 ± 13*	29.32
BS′-58	30.75	CT	*1.54*	*−6.47*			
BS′-58′	31.3	CT	*1.57*	*−6.36*	−25.47	*0.709776 ± 12*	27.04
BS′-59	31.95	CT	*1.60*	*−6.42*			
BS′-60	32.8	CT	*1.64*	*−6.43*	−27.69		29.33
BS′-61	33.3	CT	*1.60*	*−6.67*		*0.708407 ± 13*	
BS′-62	34	CT	*2.01*	*−6.33*	−27.80	*0.708766 ± 13*	29.81
BS′-63	34.32	NL	*2.06*	*−5.88*	−27.18		29.24
BS′-64	34.58	NL	*2.02*	*−6.33*	−25.46	*0.708578 ± 13*	27.48
BS′-65	34.9	NL	*2.19*	*−6.09*	−26.65		28.84
BS′-66	35.25	NL	*2.08*	*−6.27*	−25.13		27.21
BS′-67	35.55	NL	*2.03*	*−6.26*	−25.59	*0.708859 ± 13*	27.62

Stable isotope data are reported in per mil relative to VPDB, $\Delta^{13}C = \delta^{13}C_{carb} - \delta^{13}_{Corg}$. Sr isotopic ratios are normalized to NBS 987 standard of 0.710240. NL—nodular limestone, Sh M—shaly mudstone, CT—calciturbidite, CC—calci-conglomerate. Data in normal font were analysed at Ruhr University (Bochum), those in italics were measured at Institute of Geology and Geophysics, CAS (Beijing), and those in bold were derived from Chen et al.(2002) [11].

References

[1] G.R. McGhee, The Late Devonian Mass Extinction, New York, Columbia University Press, New York, 1996 (303pp).

[2] K. Wang, C.J. Orth, M.J. Attrep, B.D.E. Chatterton, H. Hou, H.H.J. Geldsetzer, Geochemical evidence for a catastrophic biotic event at the Frasnian/Famennian boundary in south China, Geology 19 (1991) 776–779.

[3] M.M. Joachimiski, W. Buggisch, Anoxic events in the late Frasnian—causes of Frasnian–Famennian faunal crisis? Geology 21 (1993) 675–678.

[4] T.J. Algeo, R.A. Berner, J.B. Maynard, S.E. Scheckler, Late Devonian oceanic anoxic event and biotic crisis: 'rooted' in the evolution of land vascular plants?, GSA Today 5 (45) (1995) 64–66.

[5] T.J. Algeo, S.E. Scheckler, Terrestrial-marine teleconnections in the Devonian: links between the evolution of land plants, weathering processes, and marine anoxic events, Philos. Trans. R. Soc., Lond. B353 (1998) 113–717.

[6] A.E. Murphy, B.B. Sageman, D.J. Hollander, Eutrophication by decoupling of the marine biogeochemical cycles of C, N, and P: a mechanism for the Late Devonian mass extinction, Geology 28 (2000) 427–430.

[7] J.B. Thompson, C.R. Newton, Late Devonian Mass Extinction: Episodic Climatic Cooling or Warming, in: N.J. McMillian, et al., (Eds.), Devonian of the World: Canad. Soc. Petrol. Geol. Mem., vol. 14, 1988, pp. 29–34.

[8] M.M. Joachimski, W. Buggisch, Conodont apatite $\delta^{18}O$ signatures indicate climatic cooling as a trigger of the Late Devonian mass extinction, Geology 30 (2002) 711–714.

[9] M.M. Joachimski, R.D. Pancost, K.H. Freeman, C. Ostertag-Henning, W. Buggisch, Carbon isotope geochemistry of the Frasnian–Famennian transition, Palaeogeogr. Palaeoclimatol. Palaeoecol. 181 (2002) 91–109.

[10] K. Wang, H.H.J.K. Geldsetzer, W.D. Goodfellow, H.R. Krouse, Carbon and sulfur isotope anomalies across the Frasnian–Famennian extinction boundary, Alberta, Canada, Geology 24 (1996) 187–191.

[11] D. Chen, M.E. Tucker, Y. Shen, J. Yans, A. Preat, Carbon isotope excursions and sea-level change: implications for the Frasnian–Famennian biotic crisis, J. Geol. Soc. (Lond.) 159 (2002) 623–626.

[12] M.M. Joachimski, C. Ostertag-Henning, R.D. Pancost, H. Strauss, K.H. Freeman, R. Littke, J.S. Sinninghe Damsté, G. Racki, Water column anoxia, enhanced productivity and concomitant changes in $\delta^{13}C$, $\delta^{34}S$ across the Frasnian–Famennian boundary (Kowala–Holy Cross Mountains/Poland), Chem. Geol. 175 (2001) 109–131.

[13] M.A. Arthur, E. Walter, L.M. Pratt, Geochemical and climatic effects of increased marine organic carbon burial at the Cenomanian/Turonian boundary, Nature 335 (1988) 714–717.

[14] K.H. Freeman, J.M. Hayes, Fractionation of carbon isotopes by phytoplankton and estimates of ancient CO_2 levels, Global Biogeochem. Cycles 6 (1992) 185–198.

[15] L.R. Kump, M.A. Arthur, Interpreting carbon-isotope excursions: carbonates and organic matter, Chem. Geol. 161 (1999) 181–198.

[16] H. Elderfield, Strontium isotope stratigraphy, Palaeogeogr. Palaeoclimatol. Palaeoecol. 57 (1986) 71–90.

[17] S.C. Clemens, J.W. Farrel, L.P. Gromet, Synchronous changes in seawater strontium isotope composition and global climate, Nature 363 (1993) 607–610.

[18] J.D. Blum, Y. Erel, A silicate weathering mechanism linking increases in marine $^{87}Sr/^{86}Sr$ with global glaciation, Nature 373 (1995) 415–418.

[19] B.L. Ingram, R. Coccioni, A. Montanari, F.M. Richter, Strontium isotopic composition of Mid-Cretaceous seawater, Science 264 (1994) 546–550.
[20] J. Veizer, B. Buhl, A. Diener, S. Ebneth, O.G. Podlaha, P. Bruckschen, T. Jasper, C. Korte, M. Schaaf, D. Ala, K. Azmy, Strontium isotope stratigraphy: potential resolution and event correlation, Palaeogeogr. Palaeoclimatol. Palaeoecol. 132 (1997) 65–77.
[21] D. Chen, M.E. Tucker, J. Zhu, M. Jiang, Carbonate sedimentation in a pull-apart basin, Middle to Late Devonian, southern Guilin, South China, Basin Res. 13 (2001) 141–168.
[22] D. Chen, M.E. Tucker, The Frasnian–Famennian mass extinction: insights from high-resolution sequence stratigraphy and cyclostratigraphy in South China, Palaeogeogr. Palaeoclimatol. Palaeoecol. 193 (2003) 87–111.
[23] H. Irwin, C. Curtis, Isotopic evidence for source of diagenetic carbonates formed during burial of organic-rich sediments, Nature 269 (1977) 209–213.
[24] J.M. Hayes, H. Strauss, A.J. Kaufman, The abundance of ^{13}C in marine organic matter and isotopic fractionation in the global biogeochemical cycle of carbon during the past 800 Ma, Chem. Geol. 161 (1999) 103–125.
[25] A.H. Knoll, J.M. Hayes, A.J. Kaufman, K. Sweet, I.B. Lambert, Secular variation in carbon isotope ratios from Upper Proterozoic successions of Svalbard and East Greenland, Nature 321 (1986) 832–838.
[26] J.M. Hayes, B.N. Popp, R. Takigiku, M. Johnson, An isotopic study of biogeochemical relationships between carbonates and organic carbon in the Greenhorn Formation, Geochim. Cosmochim. Acta 53 (1989) 2961–2972.
[27] M. Magritz, R.V. Krishamurthy, W.T. Holser, Parallel trends in organic and inorganic carbon isotopes across the Permian/Triassic boundary, Am. J. Sci. 292 (1992) 727–739.
[28] J.L. Banner, G.N. Hanson, Calculation of simultaneous isotopic and trace element variations during water–rock interaction with applications to carbonate diagenesis, Geochim. Cosmochim. Acta 54 (1990) 3123–3137.
[29] J.L. Banner, Application of the trace element and isotope geochemistry of strontium to studies of carbonate diagenesis, Sedimentology 42 (1995) 805–824.
[30] J.D. Marshall, Climatic and oceanographic isotopic signals from the carbonate rocks record and their preservation, Geol. Mag. 129 (1992) 143–160.
[31] U. Brand, Carbon, oxygen and strontium isotopes in Paleozoic carbonate components: an evaluation of original seawater-chemistry proxies, Chem. Geol. 204 (2004) 23–44.
[32] Y.M. Gong, B.H. Li, Y. Wu, Molecular fossils across the Frasnian–Famennian transition in Guangxi, Prog. Nat. Sci. 12 (2002) 182–187.
[33] M. Wilson, Z.M. Lyashkevich, Magmatism and geodynamics of rifting of the Pripyat–Dnieper–Donets rift, East European Platform, Tectonophysics 268 (1996) 65–81.
[34] G. Racki, Frasnian–Famennian biotic crisis: undervalued tectonic control? Palaeogeogr. Palaeoclimatol. Palaeoecol. 141 (1998) 177–198.
[35] V.E. Courtillot, P.R. Renne, On the ages of flood basalt events, C.R. Geoscience 335 (2003) 113–140.
[36] Y. Wu, F.L. Zhou, T.C. Jiang, D.N. Fang, W.S. Huang, The Sedimentary Facies, Palaeogeography and Relative Mineral Deposits of the Devonian in Guangxi, Guangxi People's Publishing House, Nanning, China, 1987 (292pp).
[37] G. Racki, Silica-secreting biota and mass extinctions: survival patterns and processes, Palaeogeogr. Palaeoclimatol. Palaeoecol. 154 (1999) 107–132.
[38] K.R. Hinga, M.A. Arthur, M.E.Q. Pilson, D. Whitaker, Carbonate isotope fractionation by marine phytoplankton in culture: the effects of CO_2 concentration, pH, temperature, and species, Global Biogeochem. Cycles 8 (1994) 91–102.
[39] P.B. Wignall, Large igneous provinces and mass extinction, Earth Sci. Rev. 53 (2001) 1–33.
[40] R.A. Berner, The rise of plants and their effect on weathering and atmospheric CO_2, Science 276 (1997) 544–545.
[41] M.M.M. Kuypers, R.D. Pancost, J.S. Sinningh Damsté, A large and abrupt fall in atmospheric CO_2 concentration during Cretaceous times, Nature 399 (1999) 342–345.
[42] R.A. Berner, GEOCARB II: a revised model of atmospheric CO_2 over Phanerozoic time, Am. J. Sci. 294 (1994) 56–91.
[43] C.I. Mora, S.G. Driese, P.G. Seager, Carbon dioxide in the Paleozoic atmosphere: evidence from carbon-isotope compositions of pedogenic carbonate, Geology 19 (1991) 1017–1020.
[44] C.I. Mora, S.G. Driese, L.A. Colarusso, Middle to Late Paleozoic atmospheric CO_2 levels from soil carbonate and organic matter, Science 271 (1996) 1105–1107.
[45] S.G. Driese, C.I. Mora, Physico-chemical environment of pedogenic carbonate formation in Devonian vertic palaeosols, central Appalachians, USA, Sedimentology 40 (1993) 199–216.
[46] G.H. Rau, CO_{2aq}-dependent photosynthetic ^{13}C fractionation in the ocean: a model versus measurements, Global Biogeochem. Cycles 11 (1997) 267–278.
[47] S. Burkhardt, U. Riebesell, I. Zondervan, Effects of growth rate, CO_2 concentration, and cell size on the stable carbon isotope fractionation in marine phytoplankton, Geochim. Cosmochim. Acta 63 (1999) 3729–3741.
[48] R.R. Bidigare, A. Fluegge, K.H. Freeman, K.L. Hanson, Consistent fractionation of ^{13}C in nature and in the laboratory: growth-rate effects in some haptophyte algae, Global Biogeochem. Cycles 11 (1997) 279–292.
[49] A. Clarke, Temperature and extinction in the sea: a physiologist's view, Palaeobiology 19 (1993) 499–518.
[50] P. Hallock, Fluctuations in the trophic resource continuum: a factor in global diversity cycle? Paleoceanography 2 (1987) 457–471.
[51] L.J. McCook, J. Jompa, G. Diaz-Pulido, Competition between corals and algae on coral reefs: a review of evidence and mechanism, Coral Reefs 19 (2001) 400–417.